Journal of Materials Chemistry C

Accepted Manuscript

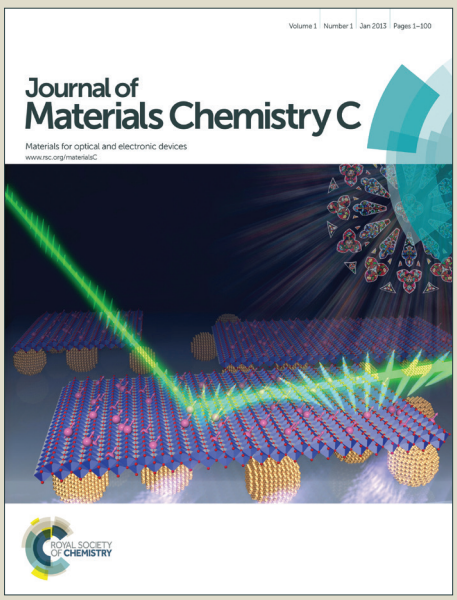

ROYAL SOCIETY OF CHEMISTRY

www.rsc.org/materialsC

Journal Name

RSCPublishing

ARTICLE

Small Molecules Incorporating Regioregular Oligothiophenes and Fluorinated Benzothiadiazole Groups for Solution-Processed Organic Solar Cells

Liu Yuan[a,b], Yifan Zhao[a,c], Kun Lv*[a], Dan Deng[a,b], Wei Yan[c], Zhixiang Wei*[a]

Cite this: DOI: 10.1039/x0xx00000x

Received 00th January 2012,
Accepted 00th January 2012

DOI: 10.1039/x0xx00000x

www.rsc.org/

Small molecules incorporating regioregular oligothiophenes and fluorinated benzothiadiazole groups have been synthesized for solution processed organic solar cells. The lengths of oligothiophene units showed profound influences on the light absorption, energy levels, crystalline behaviors and active layer morphologies. The photovoltaic performances have been tested using mixed-solvent processing method. When being blended with [6,6]-phenyl-C71-butyric acid methyl ester ($PC_{71}BM$) as the active layer, the shorter molecule 4TA4T achieved a power conversion efficiency (PCE) of 3.81%, with an open circuit voltage (V_{oc}) of 0.83 V, a short current density (J_{sc}) of 8.02 mA cm^{-2} and a Fill Factor (FF) of 0.57. The longer molecule 6TA6T showed a lower PCE of 3.21% due to a lower V_{oc} of 0.74 V. This study provides detailed insights for the design of small molecules by subtle change of donor lengths.

Introduction

The research of solar cells has been boasted by the world energy crisis and environmental issues. With the advantages of low cost, flexible and applicable in large area, organic solar cell is one of the most promising technologies for future energy harvesting.[1-5] For more than one decade, great efforts have been made for bulk-heterojunction (BHJ) polymer solar cells. With systematic material structure design and synergistic device optimizations, their PCEs have been improved to over 9% for single active layer solar cells[6-9] and 10% for tandem solar cells.[10, 11] Small molecule based BHJ solar cells, though less studied, have also achieved high PCEs over 8%.[9, 12-14] Owing to their high purity, well-defined structures and less batch-to-batch variation,[15-17] small molecules are very good candidates both for achieving high PCEs and the investigation of relationships between molecular structures, active layer characteristics and device performances.

One advantage of small molecules over polymers is their better crystallinity which benefits charge transport and suppresses charge recombination.[18] On the other hand, it may also cause over-aggregation or discontinuous domains of donor phase.[19, 20] To achieve high PCEs in BHJ solar cells, bicontinuous phase separation in proper scale and ordered packing of molecules within each phases are equally important.[21] In polymer solar cells, this problem can be partly solved by choosing proper molecular length, *i.e.* molecular weight (MW). In the case of semi-crystalline polymer P3HT, low MW P3HT can form highly crystalline regions, while high MW P3HT tends to tangle together which is beneficial for interconnection of donor domains.[22, 23] When applied in BHJ solar cells, increasing MW of P3HT can lead to higher PCEs, but this efficiency enhancement effect ends at a certain point.[24-26] Ma *et al.* found that an optimal ratio of 4:1 between low and high molecular weight P3HT can lead to a 'ideal morphology' comprised of highly ordered crystalline regions formed by low MW P3HT embedded and interconnected by a high MW P3HT matrix.[27] These results indicate that molecular length is an important issue in achieving effective molecular packing and proper phase separation. Considering small molecules generally have a structure scale under 10 nm, the influence of molecular length on molecular packing, phase separation and the eventual solar cell performance might be more profound.

Herein, we report the synthesis of a series of donor-acceptor-donor type small molecules, namely nTAnT (4 or 6) (Scheme 1), with similar structures but different molecular lengths, and their application in solution processing solar cells. Regioregular oligothiophenes are chosen as donor units for their structural simplicity and strong π-π stacking tendency. The benefits of regioregularity have been well demonstrated in the study of P3HT based field-effect transistors and solar cells. Compared with its region-random analogs, regioregular P3HT has well-defined molecular architecture and easier to self-organizing into ordered lamellar structures. These features result in higher charge carrier mobility, thus better device performances.[28-31] 5,6-difluoro-2,1,3-benzothiadiazole(DFBT) is chosen as the

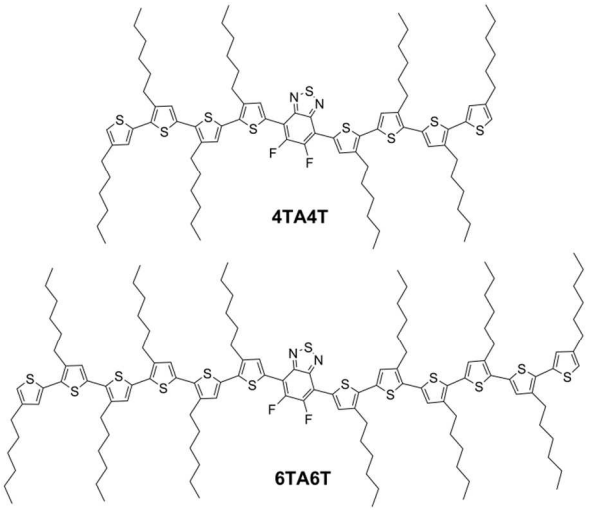

Scheme 1 Molecular structures of 4TA4T and 6TA6T

acceptor unit. DFBT is an acceptor unit widely used in polymer solar cells, and has been proved to be a better acceptor unit than its unfluorinated counterpart in most cases.[32-40] Fluorination of the acceptor units results in decreased HOMO energy levels, increased intermolecular interactions and suppressed charge recombination, leading to solar cells with enhanced performances.[41-44] As far as we know, the combination of regioregular oligothiophenes and DFBT in small molecule based solar cells has not been reported.

When being blended with $PC_{71}BM$ for solar cell applications, 4TA4T achieved a PCE of 3.8% using mixed-solvent processing method without any additives or post treatment. The longer molecule 6TA6T with elongated donor part had a lower PCE of 3.2% due to the decreasing of V_{oc}. Though photovoltaic performances of the two materials were not varied that much, their active layer morphologies were quite different, and varied with different processing solvents. Molecular length was found to have profound influences on the crystalline behaviours, phase separation properties and active layer morphologies of the two materials.

Results and discussion

Materials and synthesis

4,7-dibromo-5,6-difluoro-2,1,3-benzothiadiazole (2Br-DFBT) and (3,4'-dihexyl-[2,2'-bithiophen]-5-yl)trimethylstannane were synthesized according to reported methods.[32, 45] The synthesis of nTAnT (n = 4, 6) molecules were illustrated in Scheme 2. Starting from 2Br-DFBT, using simple Stille coupling and NBS bromination methods, nTAnT molecules can be obtained within few steps in high yield.

Thermal and solid state properties

Thermal stability of 4TA4T and 6TA6T was investigated by thermo-gravimetric (TGA) analysis. The onset temperatures with 5% weight-loss of the two molecules were over 440 °C(Fig. S1 in ESI), indicating their good thermal stability

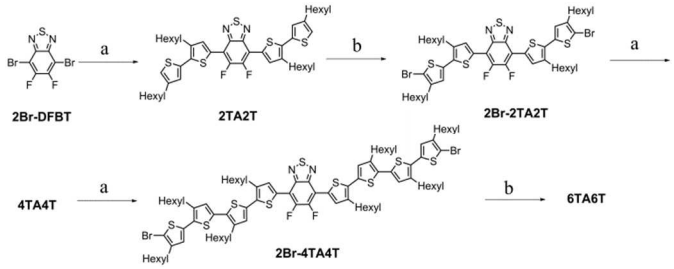

Scheme 2 Synthetic routes of 4TA4T and 6TA6T. Conditions: (a) (3,4'-dihexyl-[2,2'-bithiophen]-5-yl)trimethylstannane, Pd(PPh3)4, toluene, Ar, 115 °C, 48 h. (b) THF, NBS, 8 h.

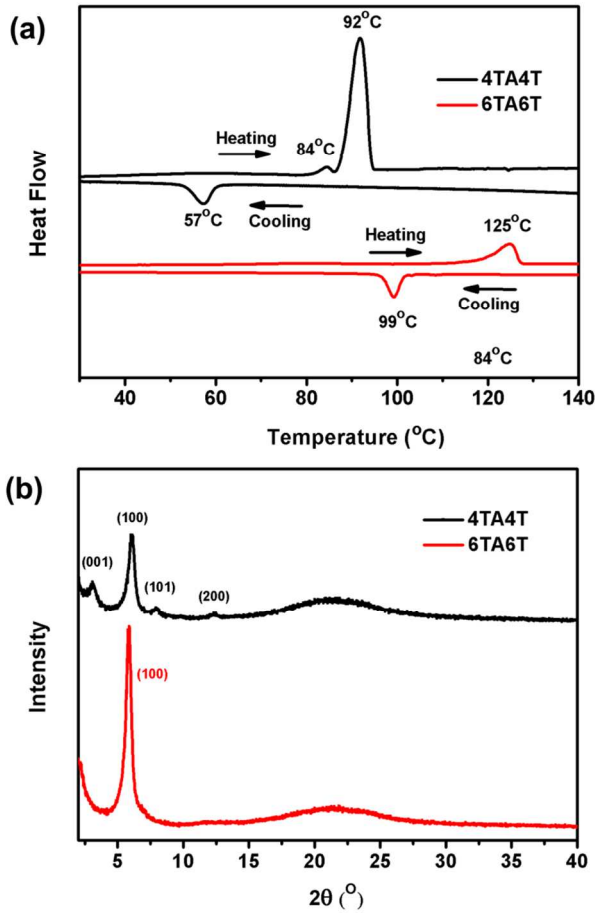

Fig. 1 (a) DSC plots of 4TA4T and 6TA6T in the 2nd scan cycles with scanning rate of 5°C min^{-1}. (b) XRD patterns of 4TA4T and 6TA6T films on glass substrate drop-casted from chloroform solutions at ambient temperature.

for the application in photovoltaic devices. Differential scanning calorimetry (DSC) analysis (Fig. 1a) showed that 4TA4T had two endothermic peaks at 84 °C and 92 °C upon heating, corresponding to the transition to mesophase and isotropic phase (melting) respectively. The mesophase transition indicates the change of molecule packing. 6TA6T had only one endothermic peak at 125 °C corresponding to the melting transition. The higher melting point is due to higher molecular weight of 6TA6T. Their exothermic peaks appeared at 57 °C and 99 °C for 4TA4T and 6TA6T respectively, which are ascribed to crystallization upon cooling.

The solid state properties of 4TA4T and 6TA6T were further studied by X-ray diffraction (XRD) analysis (Fig. 1b). The drop-casted film of 6TA6T showed a (100) peak at 2θ = 5.8°, corresponding to a d-spacing of 1.52 nm, which was originated from lamellar packing in the side chain direction. Comparing with the reported d-spacing of 1.62-1.67 nm for regioregular P3HT lamellar packing,[46, 47] the smaller d-spacing of 6TA6T indicates intercalation of the side chains. For 4TA4T films, d-spacing of the (100) peak was 1.45 nm, even smaller than that of 6TA6T. A second-order diffraction at 2θ = 12.3° corresponding to (200) peak was found for 4TA4T. Two other peaks at 2θ = 3.1° and 8.0° were also observed, which are ascribed to (001) and (101) peaks, respectively. These findings show that 4TA4T has more condensed side chain intercalation and higher molecular order than 6TA6T in the solid state.

Optical and electrochemical properties

To study the influences of molecular length on optical and electrochemical properties, two other nTAnT analogs (n = 1, 3) were also synthesized (Scheme S1 in ESI). 2TA2T is an intermediate for the synthesis 4TA4T. The UV-vis absorption spectra of nTAnT (n = 1, 2, 3, 4, 6) chloroform (CF) solutions and films are shown in Fig. 2 and Table 1. Two typical peaks were found in the spectra for all the materials, of which the high energy peak was assigned to π-π* transition and the low energy peak was caused by intra-molecular charge transfer (ICT). In both solutions and thin films, with the donor becoming longer, both peaks showed bathochromic shift due to the increase of conjugation length. In addition, the absorption coefficient of the two peaks increased continuously. Compared with the $CHCl_3$ solutions, light absorption of the films were bathochromically shifted with a shoulder appearing on the ICT peak, indicating effective π-π stacking in the solid state. From solution to film, the absorption onset of 6TA6T film was red-shifted about 70 nm, while the red-shift for 4TA4T was about 100 nm with a more evident shoulder peak, indicating a more condensed packing between the molecules in 4TA4T than that in 6TA6T.

The energy levels of the nTAnT molecules were measured by cyclic voltammetry (Fig. 3), and the results were listed in Table 1. The HOMO energy levels increased continuously with the extended molecular lengths, while the LUMO energy levels had no obvious change from 2TA2T to 6TA6T. The HOMO and LUMO energy levels of 4TA4T and 6TA6T were -5.17 eV, -3.24 eV and -5.07 eV, -3.21 eV respectively, calculated from the oxidation and reduction onset potential against Ag^+/Ag.[48] The elongation of the donor part from 4TA4T to 6TA6T resulted in 0.1 eV increase of the HOMO energy level. This may deduce the decrease of V_{oc} in organic solar cells, for V_{oc} is generally decided by the energy difference between HOMO of the donor material and LUMO of the acceptor material.[3, 49] The optical band gaps of 4TA4T and 6TA6T films were calculated from the onset of the absorption spectra to be 1.72 eV and 1.70 eV respectively. The two materials have suitable energy levels for application in solar cells with $PC_{71}BM$.

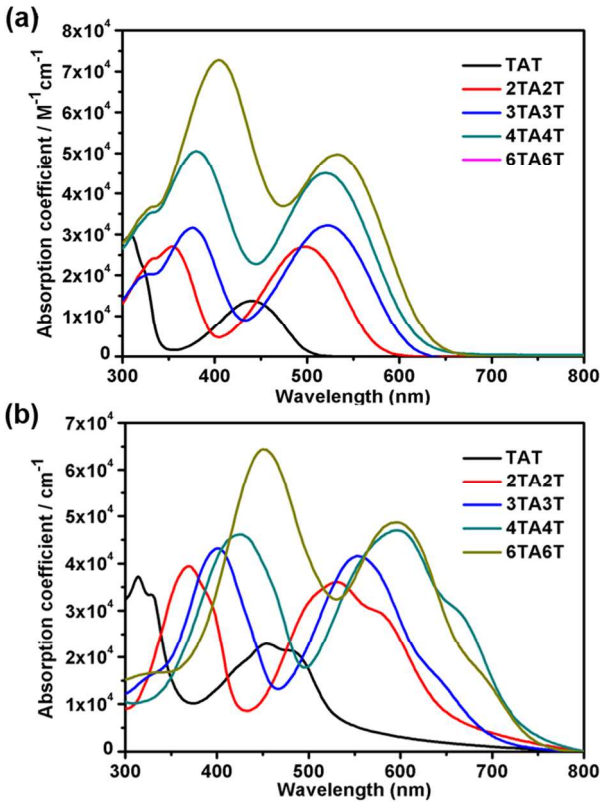

Fig. 2 UV-vis absorption spectra of nTAnT (a) in chloroform and (b) thin films.

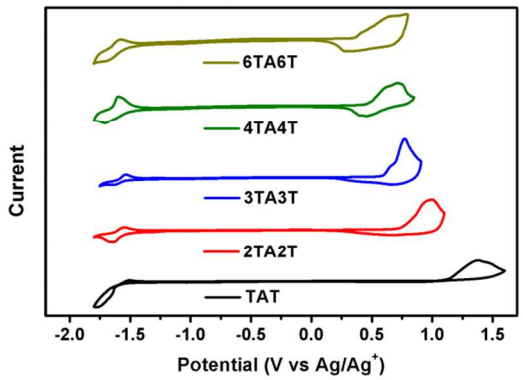

Fig. 3 Cyclic voltammograms of nTAnT films in 0.10mol L^{-1} Bu_4NPF_6 acetonitrile solution.

Photovoltaic properties

Photovoltaic devices using a structure of ITO/PEDOT:PSS /Active layer/Ca/Al were fabricated, in which the active layer was a blend of 4TA4T or 6TA6T with $PC_{71}BM$ as donor (D) and acceptor (A) materials, respectively. Two solvents CF and chlorobenzene (CB) were tried, with systematic investigation of D/A weight ratio and spin coating speed. For 4TA4T, the best D/A ratio was found at 1.5:1, with PCEs of 2.17 % and 2.75 % for CF and CB respectively (Table 2). While for 6TA6T, the best D/A ratio was 1:1, with PCEs of 1.97 % and 2.15 % for CF and CB respectively (Table S1).

Table 1 Optical and electrochemical properties of compounds nTAnT

	In Chloroform		In Film					
	λ_{max} (nm)	ε (10^4 $M^{-1}cm^{-1}$)	λ_{max} (nm)	ε (10^4 cm^{-1})	λ_{onset} (nm)	E_g^{opt} (eV)	HOMO (eV)	LUMO (eV)
TAT	308, 439	2.96, 1.41	314, 454	3.72 ,2.28	532	2.33	-5.84	-3.13
2TA2T	354, 497	2.72, 2.70	369, 528	3.95 ,3.61	645	1.92	-5.47	-3.21
3TA3T	375, 520	3.22, 3.20	400, 553	4.32 ,4.17	699	1.77	-5.27	-3.25
4TA4T	380, 521	5.04, 4.51	425, 595	4.64 ,4.69	722	1.72	-5.17	-3.24
6TA6T	404, 532	7.28, 4.98	451, 596	6.45 ,4.86	729	1.70	-5.07	-3.21

Table 2 Photovoltaic performances of 4TA4T: PC71BM BHJ solar cells under AM 1.5 G simulated solar illumination with different processing solvents

Solvents		D/A Ratio	V_{oc} (V)	J_{sc} (mA cm^{-2})	FF	PCE (%)
CB/CF	1:0	1.5:1	0.85	6.48	0.50	2.75
CB/CF	20:1	1.5:1	0.83	6.56	0.54	2.93
CB/CF	10:1	1.5:1	0.83	7.29	0.54	3.27
CB/CF	7:1	1.5:1	0.83	8.02	0.57	3.81
CB/CF	6:1	1.5:1	0.83	7.38	0.53	3.20
CB/CF	4:1	1.5:1	0.81	6.46	0.54	2.81
CB/CF	1:1	1.5:1	0.80	6.52	0.52	2.72
CB/CF	1:4	1.5:1	0.81	6.17	0.46	2.33
CF	0:1	1.5:1	0.82	6.35	0.42	2.17

Thermal annealing and the adding of 1,8-diiodooctane were found to be not helpful in enhancing the solar cell performance. Further improvement of the PCE was achieved by using mixed-solvent processing method, combining CB and CF as the processing solvent. Photovoltaic performances of 4TA4T with different processing solvents were summarized in Table 1. When CB/CF ratio changed from 20:1 to 7:1, Jsc increased from 6.17 mA cm^{-2} to 8.02 mA cm^{-2} and FF increased from 0.53 to 0.57, while Voc kept constant at 0.83 V. Further change the CB/CF ratio from 7:1 to 1:4, both Jsc and FF showed a general decreasing trend. With the best CB/CF ratio around 7:1, the PCE of 4TA4T was improved to 3.81 %. Using the same method, a best CB/CF ratio for 6TA6T was found at around 3:2, with a Voc of 0.74 V, a Jsc of 7.92 mA cm-2, and a FF of 0.55, giving a PCE of 3.21 %. The mean difference of photovoltaic parameters between the two materials is their Voc, for which 6TA6T is about 0.1 V lower than 4TA4T. This is in consistent with the 0.1 eV HOMO energy level increase from 4TA4T to 6TA6T, due to the elongation of donor unit which increases molecule electron density. Despite the difference in light absorption spectra, EQE spectra (Fig. 4b) of the two molecules are quite similar. The integrated current densities from EQE curves under AM1.5G solar spectrum agree well with that obtained from J-V curves, with variations below 5%.

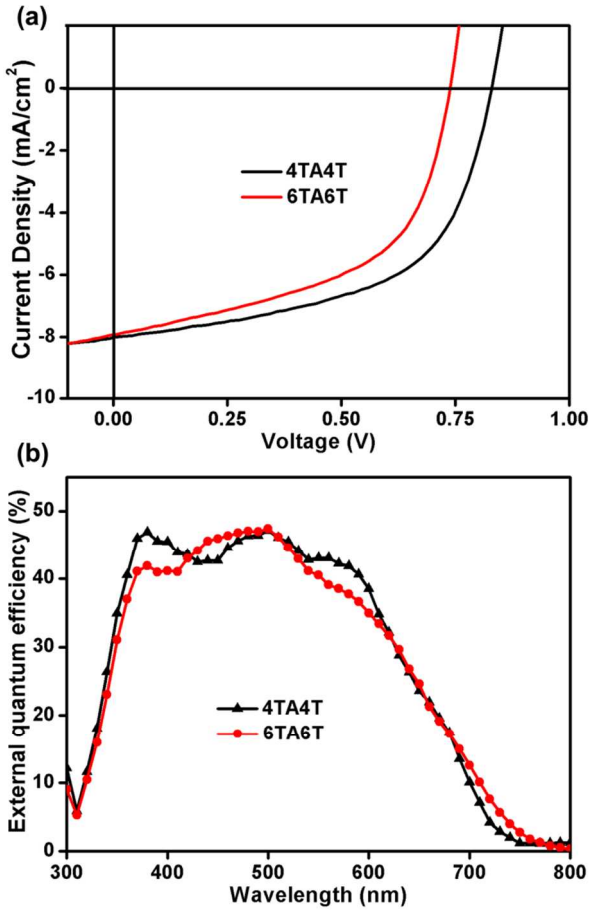

Fig. 4 (a) J-V curves of 4TA4T:$PC_{71}BM$ 1.5:1 and 6TA6T:$PC_{71}BM$ 1:1 solar cells processed using mixed solvent of CB/CF with ratio of 7:1 and 3:2 respectively and (b) their corresponding EQE curves.

Charge Carrier Mobility

The hole mobilities of 4TA4T and 6TA6T pristine films and solar cell active layers were measured by space-charge-limited current (SCLC) method, and the results were shown in Table 3 (curves are given as Figure S2 in ESI). The measured hole mobilities for pristine 6TA6T and 4TA4T were 1.83×10^{-4}

Table 3 SCLC measured hole mobilities for 4TA4T and 6TA6T and their blends with $PC_{71}BM$

	Processing solvent	Film thickness	Hole mobility ($cm^2V^{-1}S^{-1}$)
4TA4T	CF	115nm	4.82×10^{-4}
6TA6T	CF	118nm	1.83×10^{-4}
4TA4T:$PC_{71}BM$	CF	142nm	2.56×10^{-4}
	CB:CF	135nm	1.81×10^{-4}
6TA6T:$PC_{71}BM$ 1:1	CF	176nm	2.53×10^{-5}
	CB:CF	155nm	5.25×10^{-5}

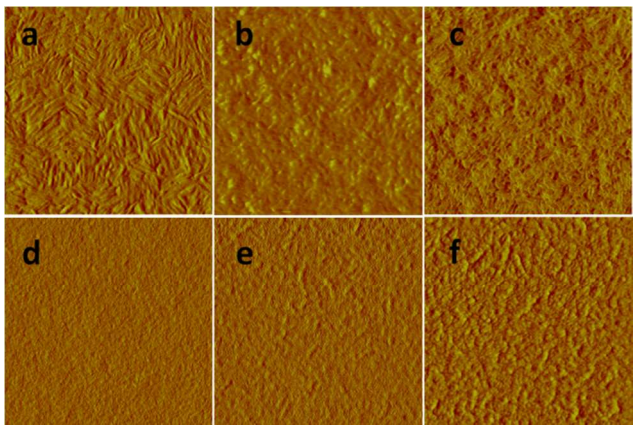

Fig. 5 AFM phase images of solar cell active layers of 4TA4T processed with (a) CF, (b) CB, (c) CB/CF 7:1 and 6TA6T processed with (d) CF, (e) CB, (f) CB/CF 3:2. All the image scales are 2μm×2μm.

$cm^2V^{-1}S^{-1}$ and 4.82×10^{-4} $cm^2V^{-1}S^{-1}$ respectively, and the latter was 2.6 times higher than the former. This is in good consistency with the DSC and XRD investigations which show better crystallinity for 4TA4T. When blended with $PC_{71}BM$, both materials showed reduced mobilities, of which 4TA4T was still 10 and 3.4 times higher than 6TA6T for CF and mixed solvent processed films, respectively. In addition, processing solvents had different influences on the blends based on two molecules. Changing the processing solvent from CF to CB:CF, 4TA4T:$PC_{71}BM$ showed reduced mobility, while the mobility of 6TA6T:$PC_{71}BM$ increased.

Film Morphology

To understand the effect of different processing solvents on charge carrier mobility and solar cell performance, AFM analysis was performed on the active layers. Fig. 5 shows the AFM phase images of CF, CB and mixed solvent processed active layers, and corresponding height images are shown as Fig. S3 in ESI. Morphologies active layers of 4TA4T and 6TA6T being processed by CF showed significant differences, the former displayed large fibrillar structures with a size of 200-300 nm and a root mean square (RMS) roughness of 1.28 nm, while the latter had a very smooth surface with a smaller RMS roughness of 0.87 nm. We deduce the big fibrillar structures of 4TA4T are caused by its good crystallinity. But this renders a bad miscibility between 4TA4T and $PC_{70}BM$ and the over-large structures cause the lack of interfaces for exciton dissociation which limits its FF and J_{sc}. Though 6TA6T has a lower packing trend, the smooth morphology and small RMS roughness value indicates a lack of phase separation and obscured D-A interfaces that breaks charge transport pass ways, resulting in low FF and J_{sc}.

When CB was used instead of CF, the big fabrillar structures in 4TA4T active layer disappeared. Smaller domains with a size of *ca.* 100 nm appeared and the RMS roughness increased from 1.28 nm to 2.05 nm. Mixed solvent further optimized the morphology of 4TA4T active layer into smaller fibril like domains and the RMS roughness increased to 2.39 nm. These morphological optimization brings more proper domain sizes and better phase separation in active layer, consequently higher J_{sc} and FF. The reduced hole mobility of CB:CF processed films than CF processed films could be ascribed to reduction of donor phase domain sizes.

For 6TA6T, the change of processing solvents from CF to CB increased the domain size while the change of RMS roughness was not evident (from 0.87 nm to 0.99 nm). Significant increase of RMS roughness (from 0.99 nm to 1.85 nm) and more apparent domains appeared when mixed solvent was used. This indicates that mixed solvent has improved the phase separation of 6TA6T active layer, providing better charge transport pass ways and reducing recombination caused by over-mixing. These effects results in the higher hole mobility and better solar cell performance for mixed solvent devices.

Conclusions

Two small molecules combining regioregular oligothiohenes and difluorinated benzothiadiazole were synthesized and incorporated in solution processed solar cells with $PC_{71}BM$, showing PCEs of 3.8% and 3.2% respectively. The elongation of the short molecule 4TA4T into 6TA6T caused 0.1 V drop of V_{oc} due to increased HOMO energy level. Mixed-solvent processing incorporating chloroform and chlorobenzene was found to be effective in optimizing active layer morphology and improve solar cell performance. Though the two molecules have very similar structures, molecular length has a significant influence on their crystalline behaviours and active layer morphology. The results illustrate that molecular length has a profound influence on small molecule solar cells performances just like in polymer solar cells.

Experimental

Measurements and characterization

^1H NMR，^{19}F NMR and ^{13}C NMR spectra were obtained on a Bruker DMX-400 NMR Spectrometer operating at 400, 377 and 101 MHz respectively, using $CDCl_3$ as solvent. MS spectra were recorded on a Micromass GCT-MS spectrometer. Thermo-gravimetric analysis was performed on a PerkinElmer Diamond TG/DTA analyzer under a nitrogen flow with a heating rate of 10 °C min^{-1}. Differential Scanning Calorimetry measurements were performed on a PerkinElmer Diamond DSC analyzer under purified nitrogen gas flow with a heating

rate of 5 °C min^{-1}. UV–Vis spectra were obtained with a JASCO V-570 spectrophotometer. X-ray diffraction measurements were carried out in the reflection mode at room temperature using a 12-Kw D/max-rA X-ray diffraction system. The step size for all scans was 4° with a count time of 1min per step. The electrochemical cyclic voltammetry was conducted on an electrochemical workstation (VMP3 Biologic, France) with Pt disk coated with the small molecule film, Pt plate, and Ag/Ag^+ electrode as working electrode, counter electrode and reference electrode respectively in a 0.1 mol L^{-1} tetrabutylammonium phosphorus hexafluoride (Bu_4NPF_6) acetonitrile solution. Atomic force microscopy (AFM) images of the blend films prepared the same way of solar cell devices were obtained on a VEECO Dimension 3100 atomic force microscope working under tapping mode.

Device fabrication and testing

ITO coated glass substrates were cleaned in deionized water, acetone and isopropyl alcohol for 10min sequentially in ultrasonic bath. After dried in nitrogen flow, the substrates were treated with oxygen plasma for 15 min. Then a 40 nm thick layer of PEDOT:PSS was spin coated onto the substrate, and dried at 150 °C for 15 min in air. The substrates were transferred into a glove-box with nitrogen atmosphere, and thin films of active layer were spin-coated from a solution of nTAnT: $PC_{71}BM$ blend CF, CB or mixed solvents, with donor material concentration of 10 mg ml^{-1}. The substrates were then transferred to a vacuum thermal evaporator, followed by deposition of the Ca/Al (20 nm/100 nm) cathode at a pressure of 2×10^{-6} Torr through a shadow mask. The current density-voltage (J-V) curves were obtained by a Keithley 2420 Source-Measure Unit. The photocurrent was measured under illumination using an Oriel Newport 150W Solar simulator (AM 1.5G). The EQE measurements of the devices were performed with an Oriel Newport System (Model 66902). All the measurements were performed at room temperature in air. Hole mobility was measured using space-charge limited current (SCLC) model. The hole only devices were fabricated in a configuration of ITO/PEDOT:PSS (35 nm)/active layer/MoO_3 (5 nm)/Au. Hole mobility can be calculated from the equation:

$$J = 9\varepsilon_0\varepsilon_r\mu V^2/8L^3$$

where J is the current density, L is the film thickness of active layer, μ is the hole mobility, ε_r (assume to be 3) is the relative dielectric constant of the transport medium, ε_0 is the permittivity of free space, V is the internal voltage in the device and $V = V_{appl} - V_r - V_{bi}$, where V_{appl} is the applied voltage to the device, V_r is the voltage drop due to contact resistance and series resistance across the electrodes, and V_{bi} is the built-in voltage due to the relative work function difference of the two electrodes. The dark current density-voltage curves were obtained by a Keithley 2420 Source-Measure Unit.

Synthesis

All reagents and chemical compounds were purchased from Sigma-Aldrich or Alfa-Aesar, used as received. Solvents and other common reagents were obtained from Beijing Chemical Plant. Toluene and tetrahydrofuran (THF) were freshly distilled before use.

2TA2T Compound 2Br-DFBT (0.33 g, 1 mmol), (3,4'-dihexyl-[2,2'-bithiophen]-5-yl)trimethylstannane (1.49 g, 3 mmol), and toluene (15 ml) were added into a 25 ml three-neck round-bottom flask, followed by the addition of Pd $(PPh_3)_4$ (57.5 mg, 0.05 mmol). The reaction flask was degassed three times and purged with argon for 5 minutes, then refluxed for 48 hours at 115 °C. The reaction mixture was cooled down to room temperature, and solvent was removed by rotary evaporation. The crude product was purified by flash column chromatography on silica gel using a mixture of dichloromethane and petroleum ether (1:10) as eluent. 2TA2T was collected as red solid (0.53 g, 63%). ^{1}H NMR (400 MHz, $CDCl_3$, ppm) δ 8.11 (s, 2H), 7.11 (d, 2H), 6.96 (s, 2H), 2.92-2.79 (m, 4H), 2.69-2.58 (m, 4H), 1.78-1.70 (m, 4H), 1.70-1.61 (m, 4H), 1.49-1.27 (m, 24H), 0.90 (dd, 12H). ^{19}F NMR (377 MHz, $CDCl_3$, ppm) δ -128.13. ^{13}C (101 MHz, $CDCl_3$, ppm) δ 151.12, 150.92, 148.80, 148.76, 148.72, 148.54, 148.34, 143.80, 139.49, 135.26, 135.09, 133.93, 129.09, 127.61, 120.61, 111.17, 111.08, 111.04, 31.72, 31.70, 30.57, 30.51, 30.43, 29.38, 29.32, 29.06, 22.68, 22.65, 14.11. MS (MALDI): calculated: 836.3, found: 836.3 (M^+). Elemental Anal. Calcd. for ($C_{46}H_{58}F_2N_2S_5$): C, 65.99; H, 6.98; N, 3.35. Found: C, 66.12; H, 7.54; N, 3.13.

2Br-2TA2T Compound 2TA2T (2 g, 2.4 mmol) was dissolved in a flask containing 100 mL THF, and NBS (940 mg, 5.2 mmol) was added in portions with stirring. After reacting for 8h in the dark, the mixture was poured into water and extracted with chloroform. The crude product was purified by flash column chromatography on silica gel using a mixture of dichloromethane and petroleum ether (1:20) as eluent. 2Br-2TA2T was collected as red solid (2.15 g, 90%). ^{1}H NMR (400 MHz, $CDCl_3$, ppm) δ 8.10 (s, 2H), 6.96 (s, 2H), 2.86-2.77 (t, 4H), 2.63-2.54 (t, 4H), 1.71 (m, 4H), 1.63 (m, 4H), 1.34 (m, 24H), 0.95-0.83 (m, 12H). ^{19}F NMR (377 MHz, $CDCl_3$, ppm) δ -127.76. ^{13}C (101 MHz, $CDCl_3$, ppm) δ 151.07, 150.87, 148.55, 148.29, 142.56, 139.81, 135.08, 133.82, 129.44, 126.97, 110.92, 31.69, 31.66, 30.51, 29.70, 29.58, 29.39, 29.32, 28.99, 22.69, 22.64, 14.12. MS (MALDI): calculated: 992.1, found: 992.1 (M^+). Elemental Anal. Calcd. for ($C_{46}H_{56}Br_2F_2N_2S_5$): C, 55.52; H, 5.67; N, 2.82. Found: C, 56.14; H, 5.84; N, 2.60.

4TA4T 4TA4T was synthesized using similar procedures of 2TA2T from 2Br-2TA2T and (3,4'-dihexyl-[2,2'-bithiophen]-5-yl)trimethylstannane. ^{1}H NMR (400 MHz, $CDCl_3$, ppm) δ 8.12 (s, 2H), 7.11 (s, 2H), 7.02-6.95 (m, 4H), 6.91 (s, 2H), 2.94-2.86 (m, 4H), 2.85-2.70 (m, 8H), 2.67-2.56 (m, 4H), 1.80-1.59 (m, 16H), 1.49-1.21 (m, 48H), 0.96-0.81 (m, 24H). ^{19}F NMR (377 MHz, $CDCl_3$, ppm) δ -128.17. ^{13}C NMR (101 MHz, $CDCl_3$, ppm) δ 148.79, 143.68, 139.89, 139.72, 139.63, 135.48, 134.68, 134.15, 133.38, 133.25, 131.30, 131.15, 129.21, 129.09, 128.54, 127.16, 120.04, 111.16, 31.71, 30.59, 30.52, 30.41, 29.56, 29.48, 29.32, 29.27, 29.03, 22.69, 22.67, 22.66, 22.64, 14.15, 14.13, 14.12. MS (MALDI): calculated: 1500.6, found: 1500.4 (M^+). Elemental Anal. Calcd. for ($C_{86}H_{114}F_2N_2S_9$): C, 68.75; H, 7.65; N, 1.86. Found: C, 69.04; H, 7.67; N, 1.96.

2Br-4TA4T 2Br-4TA4T was synthesized using similar procedures of 2Br-2TA2T from 4TA4T. ^{1}H NMR (400 MHz, $CDCl_3$, ppm) δ 8.13 (s, 2H), 7.11 (s, 2H), 6.98 (s, 2H), 6.83 (s, 2H), 2.95-2.85 (m, 4H), 2.85-2.76 (m, 4H), 2.76-2.66 (m, 4H), 2.63-2.51 (m, 4H), 1.81-1.57 (m, 16H), 1.50-1.21 (m, 48H), 1.00-0.81 (m, 24H). ^{19}F NMR (377 MHz, $CDCl_3$, ppm) δ -128.13. ^{13}C NMR (101 MHz, $CDCl_3$, ppm) δ148.74, 142.54, 140.20, 139.92, 139.61, 135.59, 134.65, 134.13, 134.00, 133.70, 131.01, 130.07, 129.35, 128.85, 128.32, 127.16, 126.60, 111.00, 108.70, 31.82, 31.80, 31.76, 31.72, 30.61, 30.53, 30.43, 29.73, 29.67, 29.49, 29.43, 29.33, 29.02, 22.79, 22.75, 22.71, 22.68, 14.17, 14.15, 14.10. MS (MALDI): calculated: 1656.5, found: 1656.7 (M^+). Elemental Anal. Calcd. for ($C_{86}H_{112}Br_2F_2N_2S_9$): C, 62.22; H, 6.80; N, 1.69. Found: C, 62.45; H, 6.91; N, 1.65.

6TA6T 6TA6T was synthesized using similar procedures of 2TA2T from 2Br-4TA4T. ^{1}H NMR (400 MHz, $CDCl_3$, ppm) δ 8.13 (s, 2H), 7.12 (s, 2H), 6.98 (t, 8H), 6.90 (s, 2H), 2.95-2.86 (m, 4H), 2.86-2.71 (m, 16H), 2.66-2.56 (m, 4H), 1.70 (m, 24H), 1.51-1.20 (m, 72H), 0.98-0.79 (m, 36H). ^{19}F NMR (377 MHz, $CDCl_3$, ppm) δ -128.15. ^{13}C NMR (101 MHz, $CDCl_3$, ppm) δ 148.75, 143.67, 139.92, 139.82, 139.75, 139.67, 135.54, 134.63, 134.10, 133.57, 133.35, 131.19, 130.99, 130.63, 129.22, 129.03, 128.58, 128.50, 128.42, 127.13, 119.99, 31.73, 31.71, 30.58, 30.52, 30.41, 29.46, 29.37, 29.35, 29.31, 29.29, 29.03, 22.72, 22.70, 22.68, 22.67, 22.64, 14.16, 14.14, 14.12. MS (MALDI): calculated: 2165.0, found: 2166.2 (M^+). Elemental Anal. Calcd. for ($C_{126}H_{170}F_2N_2S_{13}$): C, 69.82; H, 7.91; N, 1.29. Found: C, 69.99; H, 7.94; N, 1.41.

Acknowledgements

We acknowledge the financial support of the National Natural Science Foundation of China (Grant Nos. 51373181 and 21125420), the Ministry of Science and Technology of China (Grant Nos. 2010DFB63530, 2011CB932300), and the Chinese Academy of Sciences.

Notes and references

[a] National Center for Nanoscience and Technology, Beijing 100190, China
[b] University of Chinese Academy of Science, Beijing 100049, China
[c] Department of Environmental Science and Engineering, Xi'an Jiaotong University, Xi'an 710049, PR China
*Corresponding author: e-mail: weizx@nanoctr.cn

1. C. J. Brabec, N. S. Sariciftci and J. C. Hummelen, *Adv. Funct. Mater.*, 2001, 11, 15-26.
2. S. Günes, H. Neugebauer and N. S. Sariciftci, *Chem. Rev.*, 2007, 107, 1324-1338.
3. M. C. Scharber, D. Mühlbacher, M. Koppe, P. Denk, C. Waldauf, A. J. Heeger and C. J. Brabec, *Adv. Mater.*, 2006, 18, 789-794.
4. B. C. Thompson and J. M. Fréchet, *Angew. Chem. Int. Ed.*, 2008, 47, 58-77.
5. G. Yu, J. Gao, J. C. Hummelen, F. Wudl and A. J. Heeger, *Science*, 1995, 270, 1789-1791.
6. Z. He, C. Zhong, S. Su, M. Xu, H. Wu and Y. Cao, *Nat. Photonics*, 2012, 6, 591-595.
7. S. H. Liao, H. J. Jhuo, Y. S. Cheng and S. A. Chen, *Adv. Mater.*, 2013, 25, 4766-4771.
8. S. J. Liu, K. Zhang, J. M. Lu, J. Zhang, H. L. Yip, F. Huang and Y. Cao, *J. Am. Chem. Soc.*, 2013, 135, 15326-15329.
9. J. You, L. Dou, K. Yoshimura, T. Kato, K. Ohya, T. Moriarty, K. Emery, C.-C. Chen, J. Gao and G. Li, *Nat. Commun*, 2013, 4, 1446.
10. J. You, C. C. Chen, Z. Hong, K. Yoshimura, K. Ohya, R. Xu, S. Ye, J. Gao, G. Li and Y. Yang, *Adv. Mater.*, 2013, 25, 3973-3978.
11. V. Gupta, A. K. K. Kyaw, D. H. Wang, S. Chand, G. C. Bazan and A. J. Heeger, *Sci. Rep.*, 2013, 3.
12. A. K. K. Kyaw, D. H. Wang, V. Gupta, W. L. Leong, L. Ke, G. C. Bazan and A. J. Heeger, *ACS nano*, 2013, 7, 4569-4577.
13. Y. S. Liu, C. C. Chen, Z. R. Hong, J. Gao, Y. Yang, H. P. Zhou, L. T. Dou, G. Li and Y. Yang, *Sci. Rep.*, 2013, 3, 1965.
14. J. Zhou, Y. Zuo, X. Wan, G. Long, Q. Zhang, W. Ni, Y. Liu, Z. Li, G. He and C. Li, *J. Am. Chem. Soc.*, 2013, 135, 8484-8487.
15. Y. Lin, Y. Li and X. Zhan, *Chem. Soc. Rev.*, 2012, 41, 4245-4272.
16. G. C. Welch, L. A. Perez, C. V. Hoven, Y. Zhang, X.-D. Dang, A. Sharenko, M. F. Toney, E. J. Kramer, T.-Q. Nguyen and G. C. Bazan, *J. Mater. Chem.*, 2011, 21, 12700-12709.
17. Y. Sun, G. C. Welch, W. L. Leong, C. J. Takacs, G. C. Bazan and A. J. Heeger, *Nat. Mater.*, 2012, 11, 44-48.
18. W. Shin, T. Yasuda, G. Watanabe, Y. S. Yang and C. Adachi, *Chem. Mater.*, 2013, 25, 2549-2556.
19. J. Shin, N. S. Kang, K. H. Kim, T. W. Lee, J.-I. Jin, M. Kim, K. Lee, B. K. Ju, J.-M. Hong and D. H. Choi, *Chem. Commun.*, 2012, 48, 8490-8492.
20. S. Ma, Y. Fu, D. Ni, J. Mao, Z. Xie and G. Tu, *Chem. Commun.*, 2012, 48, 11847-11849.
21. Y. Matsuo, Y. Sato, T. Niinomi, I. Soga, H. Tanaka and E. Nakamura, *J. Am. Chem. Soc.*, 2009, 131, 16048-16050.
22. K. Zhao, H. U. Khan, R. Li, Y. Su and A. Amassian, *Adv. Funct. Mater.*, 2013, 23, 6024-6035.
23. M. T. Dang, L. Hirsch, G. Wantz and J. D. Wuest, *Chem. Rev.*, 2013, 113, 3734-3765.
24. R. C. Hiorns, R. De Bettignies, J. Leroy, S. Bailly, M. Firon, C. Sentein, A. Khoukh, H. Preud'homme and C. Dagron‐Lartigau, *Adv. Funct. Mater.*, 2006, 16, 2263-2273.
25. M. Morana, P. Koers, C. Waldauf, M. Koppe, D. Muehlbacher, P. Denk, M. Scharber, D. Waller and C. Brabec, *Adv. Funct. Mater.*, 2007, 17, 3274-3283.
26. P. Schilinsky, U. Asawapirom, U. Scherf, M. Biele and C. J. Brabec, *Chem. Mater.*, 2005, 17, 2175-2180.
27. W. Ma, J. Y. Kim, K. Lee and A. J. Heeger, *Macromol. Rapid Commun.*, 2007, 28, 1776-1780.
28. Y. Kim, S. Cook, S. M. Tuladhar, S. A. Choulis, J. Nelson, J. R. Durrant, D. D. C. Bradley, M. Giles, I. Mcculloch, C. S. Ha and M. Ree, *Nat. Mater.*, 2006, 5, 197-203.
29. R. Mauer, M. Kastler and F. Laquai, *Adv. Funct. Mater.*, 2010, 20, 2085-2092.
30. Z. Bao, A. Dodabalapur and A. J. Lovinger, *Appl. Phys. Lett.*, 1996, 69, 4108-4110.
31. C. H. Woo, B. C. Thompson, B. J. Kim, M. F. Toney and J. M. J. Frechet, *J. Am. Chem. Soc.*, 2008, 130, 16324-16329.
32. L. Dou, C.-C. Chen, K. Yoshimura, K. Ohya, W.-H. Chang, J. Gao, Y. Liu, E. Richard and Y. Yang, *Macromolecules*, 2013, 46, 3384-3390.

33. J. J. Intemann, K. Yao, H.-L. Yip, Y.-X. Xu, Y.-X. Li, P.-W. Liang, F.-Z. Ding, X. Li and A. K.-Y. Jen, *Chem. Mater.*, 2013, 25, 3188-3195.
34. Y. Li, J. Zou, H.-L. Yip, C.-Z. Li, Y. Zhang, C.-C. Chueh, J. Intemann, Y. Xu, P.-W. Liang and Y. Chen, *Macromolecules*, 2013, 46, 5497-5503.
35. Z. Li, J. Lu, S.-C. Tse, J. Zhou, X. Du, Y. Tao and J. Ding, *J. Mater. Chem.*, 2011, 21, 3226-3233.
36. B. C. Schroeder, Z. Huang, R. S. Ashraf, J. Smith, P. D'Angelo, S. E. Watkins, T. D. Anthopoulos, J. R. Durrant and I. McCulloch, *Adv. Funct. Mater.*, 2012, 22, 1663-1670.
37. R. ShahidáAshraf, J. Andrew and P. ShakyaáTuladhar, *Chem. Commun.*, 2012, 48, 7699-7701.
38. N. Wang, Z. Chen, W. Wei and Z. Jiang, *J. Am. Chem. Soc.*, 2013, 135, 17060-17068.
39. Y. X. Xu, C. C. Chueh, H. L. Yip, F. Z. Ding, Y. X. Li, C. Z. Li, X. Li, W. C. Chen and A. K. Y. Jen, *Adv. Mater.*, 2012, 24, 6356-6361.
40. H. Zhou, L. Yang, A. C. Stuart, S. C. Price, S. Liu and W. You, *Angew. Chem.*, 2011, 123, 3051-3054.
41. S. Albrecht, S. Janietz, W. Schindler, J. Frisch, J. Kurpiers, J. Kniepert, S. Inal, P. Pingel, K. Fostiropoulos and N. Koch, *J. Am. Chem. Soc.*, 2012, 134, 14932-14944.
42. A. C. Stuart, J. R. Tumbleston, H. Zhou, W. Li, S. Liu, H. Ade and W. You, *J. Am. Chem. Soc.*, 2013, 135, 1806-1815.
43. Y. Zhang, J. Zou, C.-C. Cheuh, H.-L. Yip and A. K.-Y. Jen, *Macromolecules*, 2012, 45, 5427-5435.
44. H. J. Son, W. Wang, T. Xu, Y. Liang, Y. Wu, G. Li and L. Yu, *J. Am. Chem. Soc.*, 2011, 133, 1885-1894.
45. F. C. Krebs and M. Biancardo, *Sol. Energy Mater. Sol. Cells*, 2006, 90, 142-165.
46. E. Verploegen, R. Mondal, C. J. Bettinger, S. Sok, M. F. Toney and Z. Bao, *Adv. Funct. Mater.*, 2010, 20, 3519-3529.
47. R. J. Kline, M. D. McGehee, E. N. Kadnikova, J. Liu, J. M. Frechet and M. F. Toney, *Macromolecules*, 2005, 38, 3312-3319.
48. Y. Li, Y. Cao, J. Gao, D. Wang, G. Yu and A. J. Heeger, *Synth. Met.*, 1999, 99, 243-248.
49. A. Gadisa, M. Svensson, M. R. Andersson and O. Inganäs, *Appl. Phys. Lett.*, 2004, 84, 1609-1611.

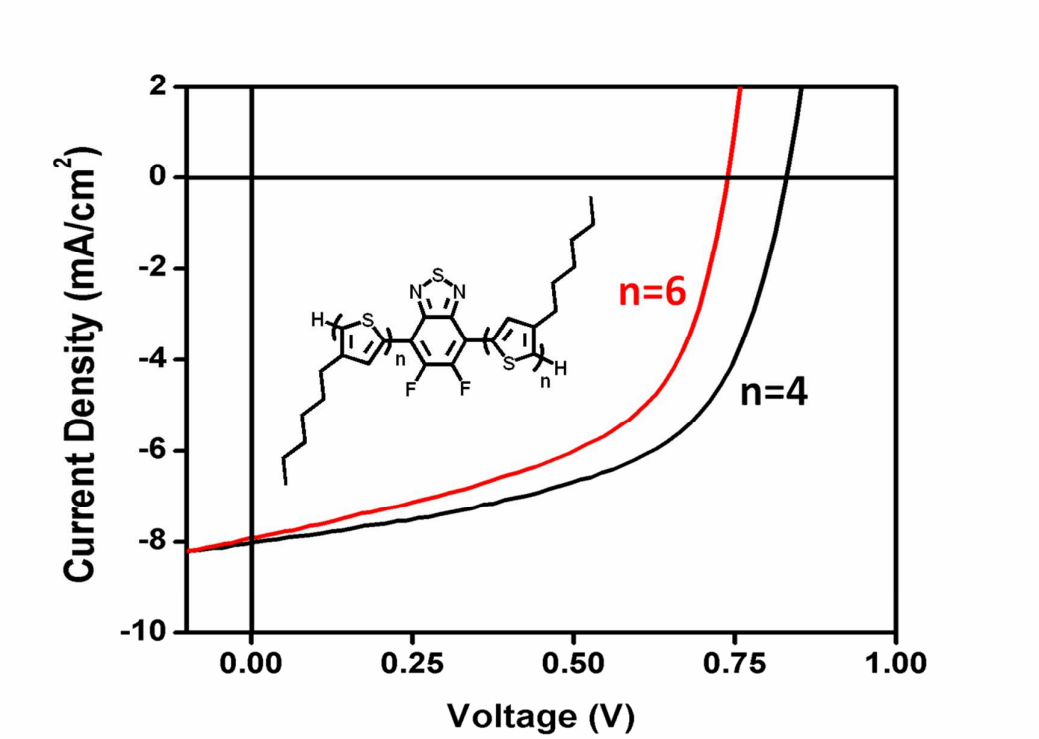

A series of donor-acceptor-donor type small molecules for solution processed solar cells by incorporating fluorinated benzothiadiazole and regioregular oligothiophenes. The influence of donor length on photovoltaic performance has been symmetrically investigated.